J. Fluid Mech. (1983), *vol.* 137, *pp.* 285–305
Printed in Great Britain

Interaction of rarefaction waves with area reductions in ducts

By J. J. GOTTLIEB AND O. IGRA†
Institute for Aerospace Studies, University of Toronto, Downsview, Ontario, Canada

(Received 17 March 1983)

The interaction of a rarefaction wave with a gradual monotonic area reduction of finite length in a duct, which produces transmitted and reflected rarefaction waves and other possible rarefaction and shock waves, was studied both analytically and numerically. A quasi-steady flow analysis which is analytical for an inviscid flow of a perfect gas was used first to determine the domains of and boundaries between four different wave patterns that occur at late times, after all local transient disturbances from the interaction process have subsided. These boundaries and the final constant strengths of the transmitted, reflected and other waves are shown as a function of both the incident rarefaction-wave strength and area-reduction ratio, for the case of diatomic gases and air with a specific-heat ratio of $\frac{7}{5}$. The random-choice method was then used to solve numerically the conservation equations governing the one-dimensional non-stationary gas flow for many different combinations of rarefaction-wave strengths and area-reduction ratios. These numerical results show clearly how the transmitted, reflected and other waves develop and evolve with time, until they eventually attain constant strengths, in agreement with quasi-steady flow predictions for the asymptotic wave patterns. Note that in all of this work the gas in the area reduction is initially at rest.

1. Introduction

The interaction of shock waves with area changes of finite length in ducts has been investigated fairly thoroughly during the past three decades, by considering the wave motion and flow as one-dimensional. This interaction process that eventually results in a well-defined quasi-steady flow (at late times) is now well understood and documented (e.g. Kahane *et al.* 1954; Rudinger 1955; Chester 1960; Russell 1967; and especially Greatrix & Gottlieb 1982). By contrast, no work of a similar nature is available for the case of a rarefaction wave interacting with an area change, although the papers by Kahane *et al.* (1954), Rudinger (1955), Schultz-Grunow (1943) and Bannister & Mucklow (1948) contain relevant basic information. Yet, the passage of a rarefaction wave through an area change is a common feature of non-stationary gas flows encountered in engineering practice and research. For example, these flows occur in the piping system of reciprocating engines and pumps, in gas-transportation pipelines, and in shock tubes and blast-wave simulators that have an area change in the driver or at the diaphragm station.

The case of a rarefaction wave (and other waves) moving in a duct with or without area changes can, of course, be handled routinely by well-developed mathematical methods. In early work the method of characteristics was employed to predict

† Present address: Ben-Gurion University of the Negev, Beer-Sheva, Israel.

non-stationary flows in ducts; for example, see the work of Bannister & Mucklow (1948) and Rudinger (1955). In this work the flow through constant-area duct segments was treated as non-stationary, and, for simplicity needed in hand calculations, the flow across each area change between constant-area segments was treated simply as steady. With the advent of high-speed computers, however, modern gasdynamic computer codes based on the method of characteristics, finite-difference methods and the random-choice method now treat the flows more realistically as non-stationary everywhere, including each gradual area change (e.g. Warming & Beam 1977; Greatrix & Gottlieb 1982; Jones & Brown 1982). These general-purpose computer codes treat any rarefaction wave interaction with an area change as an integral part of the whole flow problem. They have not been applied, however, with the specific intent of making a thorough study of such an interaction process.

The purpose of the present extensive study is to present basic detailed results that apply in general to the specific case of a rarefaction wave interacting with an area reduction. Special attention is devoted to understanding the nature of the transient flow phenomena that eventually establish a quasi-steady flow at late times, after all transient disturbances have subsided. A clear picture is thereby provided of the entire non-stationary interaction process.

2. Analytical and numerical analyses

2.1. *Quasi-steady flow analysis*

A rarefaction wave moving through a quiescent gas toward an area reduction in a duct is illustrated in figure 1. This wave produces a flow that moves in the opposite direction. Depending on the magnitudes of the area-reduction ratio S_u/S_d and the incident rarefaction-wave strength (or pressure ratio p_2/p_1 across this wave), the rarefaction-wave interaction with the area reduction will result in one of the four different postulated wave patterns shown schematically in figure 2. Transmitted and reflected rarefaction waves are shown in wave patterns A to D; an upstream-facing shock wave appears also in the area change in pattern B or downstream of it in pattern C, whereas an upstream-facing rarefaction wave appears downstream of the area change in pattern D. Owing to the existence of the shock wave in patterns B and C, a contact surface or contact region also occurs in these patterns.

The rarefaction-wave interaction with the area reduction is initially a non-stationary flow process, and the flow solution obtained from the one-dimensional equations of motion for this interaction will be numerical (see §2.2). However, as local transient disturbances subside through wave reflection and coalescing processes, the flow will become quasi-steady or steady. That is, the rarefaction and shock waves will eventually become distinct and develop constant strengths, and these waves and the contact region will eventually separate developed regions of steady flow. The solution for the quasi-steady flow for patterns A to D can be obtained analytically, and quite readily, as outlined herein.

The concept and application of a quasi-steady flow analysis are fairly well known in gasdynamics (e.g. Rudinger 1955). However, they are not presented in Rudinger's book or elsewhere in a form suitable for convenient utilization in obtaining all of the flow properties of the quasi-steady waves and steady-flow regions for patterns A to D of the present paper. Consequently, the method of solution for pattern A will be presented briefly for illustrative purposes.

For an inviscid flow of a perfect gas, the flow properties in regions 1 and 7, on either

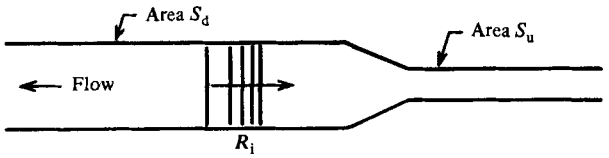

FIGURE 1. Illustration of a rarefaction wave moving toward an area reduction in a duct.

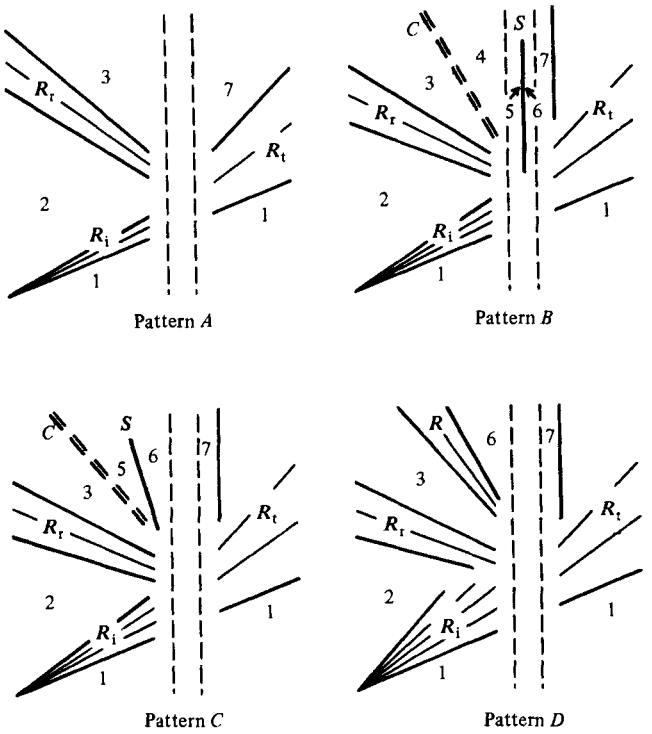

FIGURE 2. Four different schematic quasi-steady wave patterns for the interaction of a rarefaction wave with an area reduction in a duct.

side of the transmitted rarefaction wave (see pattern A in figure 2), are connected by an equation for a negatively sloped characteristic line crossing a simple expansion wave (Rudinger 1955),

$$\frac{2}{\gamma-1}a_7 - u_7 = \frac{2}{\gamma-1}a_1 \tag{1}$$

(with $u_1 = 0$), and the isentropic relations

$$\frac{p_7}{p_1} = \left(\frac{T_7}{T_1}\right)^{\gamma/(\gamma-1)} = \left(\frac{a_7}{a_1}\right)^{2\gamma/(\gamma-1)} = \left(\frac{\rho_7}{\rho_1}\right)^{\gamma}. \tag{2}$$

The symbols p, T, a, ρ, u and γ denote static pressure, temperature, sound speed, density, flow velocity and specific-heat ratio respectively. If the strength of the transmitted rarefaction wave p_7/p_1 is specified for convenience instead of p_2/p_1 of the incident rarefaction wave, all of the flow properties in region 7 can then be obtained directly from (1) and (2), because the flow properties in region 1 are known initial conditions. Note that the flow velocity in region 1 is taken to be zero in the present work.

For a steady one-dimensional isentropic flow through the area reduction, from region 7 to region 3, the continuity and energy equations (Rudinger 1955)

$$\rho_3 u_3 S_d = \rho_7 u_7 S_u, \tag{3}$$

$$h_3 + \tfrac{1}{2}u_3^2 = h_7 + \tfrac{1}{2}u_7^2, \tag{4}$$

along with the sound-speed relation $a^2 = \gamma RT = \gamma p/\rho$, and the enthalpy $h = C_p T = \gamma RT/(\gamma - 1)$, yield

$$\frac{p_3}{p_7} = \left(\frac{T_3}{T_7}\right)^{\gamma/(\gamma-1)} = \left(\frac{a_3}{a_7}\right)^{2\gamma/(\gamma-1)} = \left(\frac{\rho_3}{\rho_7}\right)^{\gamma}$$
$$= \left(\frac{M_7 S_u}{M_3 S_d}\right)^{2\gamma/(\gamma+1)} = \left(\frac{2+(\gamma-1)M_7^2}{2+(\gamma-1)M_3^2}\right)^{\gamma/(\gamma-1)}. \tag{5}$$

The symbols h, R and M denote the specific enthalpy, gas constant and flow Mach number u/a, respectively. Because M_7 is dictated by previously determined information (u_7 and a_7) and the duct cross-sectional areas upstream (S_u) and downstream (S_d) of the area reduction are specified, M_3 can be obtained from the latter part of (5). Values for p_3, T_3, a_3, and ρ_3 then follow from the former part of (5), and u_3 is obtained from the product $a_3 M_3$.

Region 2 lies behind the incident rarefaction wave and ahead of the reflected rarefaction wave (see pattern A in figure 2). The flow properties in this region are connected to region 1 by an equation for a negatively sloped characteristic line,

$$\frac{2}{\gamma-1}a_2 - u_2 = \frac{2}{\gamma-1}a_1, \tag{6}$$

and to region 3 by a similar equation for a positively sloped characteristic line,

$$\frac{2}{\gamma-1}a_2 + u_2 = \frac{2}{\gamma-1}a_3 + u_3. \tag{7}$$

These two equations yield a_2 and u_2, and p_2, T_2 and ρ_2 then follow from a set of isentropic expressions like those given by (2). This completes the method of solution for obtaining all flow properties and wave strengths for pattern A.

The procedure for obtaining a complete set of flow properties for wave patterns A to D, for some specific area-reduction ratio, is now outlined. The solution for pattern A covers a limited range of strengths of the incident and transmitted rarefaction waves. For the transmitted wave, the ratio p_7/p_1 takes on values from unity, for which there is no flow and all waves are Mach waves, to a minimum value of $\{p_7/p_1\}_{\min} = (2/\{\gamma+1\})^{2\gamma/(\gamma-1)}$, when the transmitted wave is strongest. At $\{p_7/p_1\}_{\min}$ the tail of the transmitted rarefaction wave has become vertical, as shown in pattern B of figure 2, and the flow entering the area change from region 7 is just sonic with $M_7 = -1$. For pattern A, the pressure ratio p_7/p_1 is first decreased in small increments from unity to its minimum value $\{p_7/p_1\}_{\min}$, and the flow properties in regions 2 and 3 are then calculated at each step by using the previously described method and equations. Note that if p_7/p_1 is specified, the flow properties in regions 2, 3 and 7 (including p_2/p_1) can be obtained directly, whereas, if p_2/p_1 was specified initially, the flow properties (including p_7/p_1) could be determined only by iteration.

For pattern B, an upstream-facing shock wave with a strength p_5/p_6 greater than unity is stationary in the area change. For the analysis its location can be changed in small increments from the smallest area S_u where $p_5/p_6 = 1$ to the largest area S_d

where $p_5/p_6 = \{p_5/p_6\}_{\max}$. This procedure is again convenient to obtain the flow properties (including p_2/p_1) without an iteration. The sudden change in the flow properties across this stationary shock wave, from supersonic to subsonic flow conditions, has to be included in the calculations by using the well-known Rankine–Hugoniot relations (Rudinger 1955). The flow properties in regions 2, 3 and 4 of pattern B are then calculated in a manner similar to that for pattern A. The contact surface separating regions 3 and 4 is handled easily because both the pressure and flow velocity are unchanged across it.

For pattern C, an upstream-facing shock wave that is swept downstream by the oncoming supersonic flow occurs with a contact surface swept downstream of the area change. In the calculations the strength p_5/p_6 of this downstream-swept shock wave is reduced in small increments from its maximum value $\{p_5/p_6\}_{\max}$ to its minimum values of unity when this shock wave becomes a Mach wave. The flow-property changes across this shock wave and the velocity at which it is swept downstream follow directly from the Rankine–Hugoniot relations.

Finally, for pattern D, an upstream-facing rarefaction wave that is swept downstream by the oncoming supersonic flow replaces the downstream-swept shock wave, and a contact surface does not appear. In the calculations the strength p_3/p_6 of this downstream-swept rarefaction wave is reduced incrementally from its upper value of unity, for the case of a Mach wave, to its minimum value of zero, for which this rarefaction wave is strongest. The flow-property changes across this downstream-swept rarefaction wave are obtained by using expressions like those given by (1) and (2). Note that, if p_3/p_6 is reduced to zero, p_2/p_1 also goes to zero, and the incident rarefaction wave becomes a complete expansion wave with its fan of characteristics spread out to the maximum extent. It would then be much wider spread than sketched in pattern D of figure 2.

From the previous comments it should be clear that the boundaries between patterns A, B, C and D are defined in the following manner. For the boundary between patterns A and B, the tail of the transmitted rarefaction wave of pattern A becomes vertical, and the flow in region 7 which enters the area change becomes sonic ($M_7 = -1$), whereas the stationary shock wave of pattern B is only a Mach wave at the flow entrance to the area change (S_u). For the boundary between patterns B and C, the stationary shock wave of pattern B and the downstream-swept shock wave of pattern C become stationary at the flow exit of the area change (S_d), where they have the same strength. Finally, for the boundary between patterns C and D, the downstream-swept shock and rarefaction waves of patterns C and D respectively become Mach waves. Hence, at each boundary the adjacent wave patterns have the same limiting pattern.

2.2. *Non-stationary flow analysis*

The continuity, momentum and energy equations for one-dimensional non-stationary inviscid gas flows, in conservation form, are (Rudinger 1955)

$$\frac{\partial}{\partial t}(\rho)+\frac{\partial}{\partial x}(\rho u) = -\frac{1}{S}\frac{\mathrm{d}S}{\mathrm{d}x}(\rho u), \tag{8}$$

$$\frac{\partial}{\partial t}(\rho u)+\frac{\partial}{\partial x}(\rho u^2+p) = -\frac{1}{S}\frac{\mathrm{d}S}{\mathrm{d}x}(\rho u^2), \tag{9}$$

$$\frac{\partial}{\partial t}(e)+\frac{\partial}{\partial x}(ue+up) = -\frac{1}{S}\frac{\mathrm{d}S}{\mathrm{d}x}(ue+up), \tag{10}$$

where the new symbols x, t, S and e denote distance, time, duct cross-sectional area and total energy per unit volume respectively. The total energy is the sum of the internal energy $\rho C_v T$ and kinetic energy $\frac{1}{2}\rho u^2$, which is often expressed as $p/(\gamma-1)+\frac{1}{2}\rho u^2$. This set of equations is completed by the thermal equation of state for a perfect gas, that is $p = \rho RT$.

For the solution of the problem of a rarefaction wave interacting with an area reduction in a duct, the specific variation of area $S(x)$ is required. In the present work the area change between two constant-area ducts of upstream area S_u and downstream area S_d is specified by

$$S(x) = S_d \exp\left(\tfrac{1}{2}\ln\left(\frac{S_u}{S_d}\right)\left(1-\cos\frac{\pi x}{l}\right)\right), \tag{11}$$

where $x = 0$ at the large end (S_d) and $x = l$ at the small end (S_u). This particular area transition is monotonic and smooth, and applies for both an enlargement and a reduction. It was chosen because

$$\frac{1}{S}\frac{\mathrm{d}S}{\mathrm{d}x} = \frac{\pi}{2l}\ln\left(\frac{S_u}{S_d}\right)\sin\frac{\pi x}{l} \tag{12}$$

is a symmetric, sinusoidal distribution, which is advantageous over asymmetrical variations in reducing numerical noise in the computed flow properties.

Equations (8)–(12) are solved numerically in the present study, by using the random-choice method (RCM) invented by Glimm (1965) and first applied by Chorin (1976), which is well suited for solving such problems. Shock waves and contact surfaces with sharp fronts are well defined by this method, unlike finite-difference methods for which they are smeared out over many mesh zones, owing to the effects of explicit artificial and implicit numerical viscosities. The operator-splitting technique introduced to the RCM by Sod (1977), in order that one-dimensional flow problems with area changes could be solved, is also used in this study. Note that the RCM is a first-order, explicit numerical scheme that repeatedly solves a Riemann or shock-tube problem between two grid points, and details of this method can be found in the work of Glimm (1965), Chorin (1976), Sod (1977) and Saito & Glass (1979).

3. Results and discussion

3.1. *Quasi-steady flow*

For a rarefaction wave interacting with an area reduction in a duct, four different wave patterns shown schematically in figure 2 were postulated. Based on the quasi-steady flow analysis presented in §2.1, the domains and boundaries for patterns A, B, C and D can be calculated as a function of the pressure ratio p_2/p_1 of the incident rarefaction wave and the area-reduction ratio S_u/S_d. The results for perfect air and diatomic gases with $\gamma = \frac{7}{5}$ are given in figure 3. Addition results are presented in figure 4 for the cases of perfect monatomic gases with $\gamma = \frac{5}{3}$ (solid lines) and a perfect polyatomic gas with $\gamma = \frac{11}{10}$ (dashed lines), in order to show the effects of different specific-heat ratios.

The boundaries for each different gas have a confluence point at the top of the graph where $S_u/S_d = 1$ and $p_2/p_1 = (2/\{\gamma+1\})^{2\gamma/(\gamma-1)}$. From this point they separate and run downward, and each one ends at a different point on the bottom of the graph

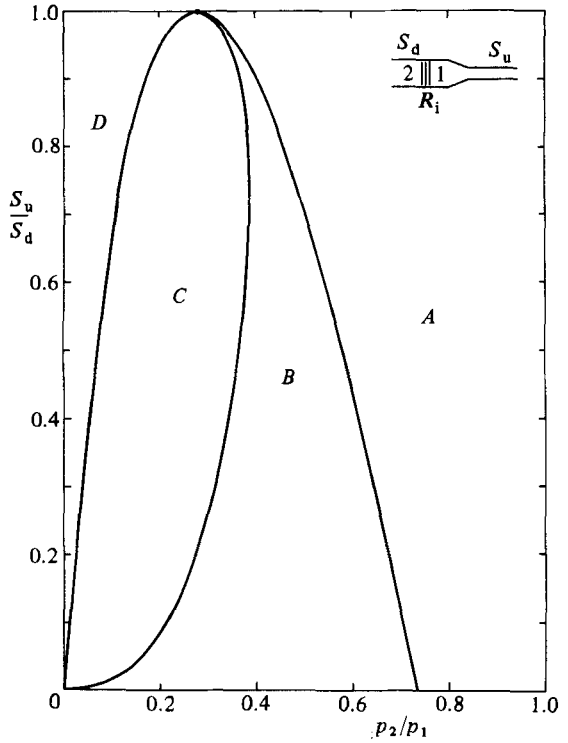

FIGURE 3. Domains and boundaries for wave patterns A, B, C and D for the interaction of a rarefaction wave of incident pressure ratio p_2/p_1 with an area reduction of ratio S_u/S_d, for the case of perfect air and diatomic gases with $\gamma = \frac{7}{5}$.

where $S_u/S_d = 0$. The values of p_2/p_1 at these three end points are

$$\left(\frac{1}{2}+\frac{1}{2}\left(\frac{2}{\gamma+1}\right)^{\frac{1}{2}}\right)^{2\gamma/(\gamma-1)}, \tag{13}$$

$$\left(\frac{1}{2}-\frac{1}{2}\left(\frac{\gamma-1}{\gamma+1}\right)^{\frac{3}{2}}\right)^{2\gamma/(\gamma-1)}, \tag{14}$$

$$\left(\frac{1}{2}-\frac{1}{2}\left(\frac{\gamma-1}{\gamma+1}\right)^{\frac{1}{2}}\right)^{2\gamma/(\gamma-1)}, \tag{15}$$

for the boundaries between patterns A and B, B and C, and C and D respectively, which can be obtained from the appropriate quasi-steady flow equations by taking the limit as $S_u/S_d \to 0$. Consequently, for any given area ratio in the range $0 \leqslant S_u/S_d < 1$, the quasi-steady flow analysis predicts that all four wave patterns can occur, depending on the incident rarefaction-wave strength p_2/p_1. For the limiting and trivial case when $S_u/S_d = 1$ (no area change), only patterns A and D are possible. For the case of pattern A the incident rarefaction wave merely becomes the transmitted wave, and no reflected wave occurs. In the case of pattern D, the first part of the incident rarefaction wave from its head (zero flow) to its 'centre' where one of its characteristic lines is vertical (sonic flow) becomes the transmitted wave, the latter part from its centre to its tail (where the flow is supersonic) becomes the

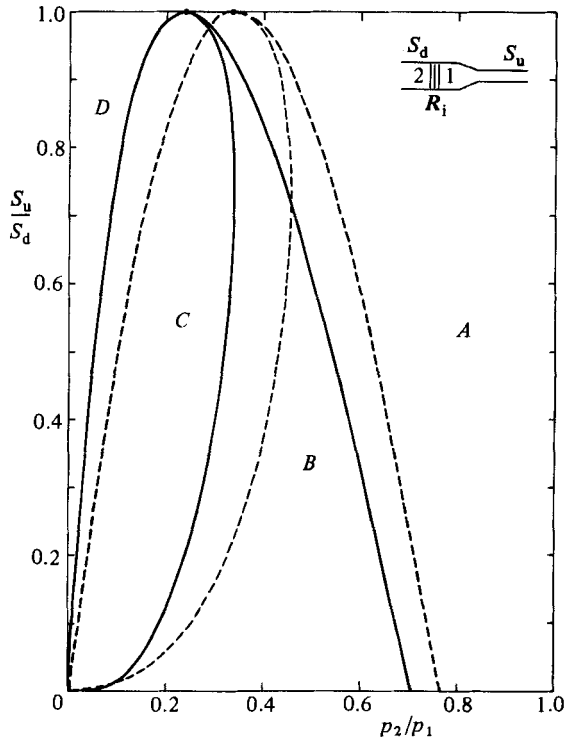

FIGURE 4. Domains and boundaries for wave patterns A, B, C and D for the interaction of a rarefaction wave of incident pressure ratio p_2/p_1 with an area reduction of ratio S_u/S_d, for the cases of perfect monatomic gases with $\gamma = \frac{5}{3}$ (——) and a perfect polyatomic gas with $\gamma = \frac{11}{10}$ (– – – –).

upstream-facing but downstream-swept rarefaction wave, and no reflected wave exists.

The strength p_7/p_1 of the transmitted rarefaction wave is shown in figure 5, in terms of the incident rarefaction-wave strength p_2/p_1 and area-reduction ratio S_u/S_d, for perfect diatomic gases and air with $\gamma = \frac{7}{5}$. Within a triangular-shaped region, corresponding to the case of wave pattern A, p_7/p_1 is a unique function of p_2/p_1 and S_u/S_d. Along the line on the left-hand side where $S_u/S_d = 1$, for the case of no area change, the strength of the transmitted rarefaction wave is, of course, equal to that for the incident rarefaction wave. For all other area-reduction ratios within the triangular region p_7/p_1 is less than p_2/p_1, showing that the transmitted rarefaction wave is stronger than the incident rarefaction wave. The transmitted wave is strongest at the right-hand side where $S_u/S_d = 0$, that is, the duct of area S_d is infinitely larger than the duct of area S_u. As p_2/p_1 is reduced from unity, for a given area ratio, p_7/p_1 decreases from unity within the triangular region and eventually reaches its lower limit of $(2/\{\gamma+1\})^{2\gamma/(\gamma-1)}$ or 0.279 (if $\gamma = \frac{7}{5}$) for the bottom border of the triangular region. Further reductions in p_2/p_1, which will produce wave patterns B, C and then D, do not alter p_7/p_1 from its lower limit, since the transmitted rarefaction wave cannot accelerate the flow beyond its sonic speed at the flow entrance to the area change. This is similar to the case of a steady flow from a constant-pressure reservoir becoming choked at the nozzle throat if the downstream pressure is lowered sufficiently.

The strength p_3/p_2 of the reflected rarefaction wave is shown in figure 6, as a

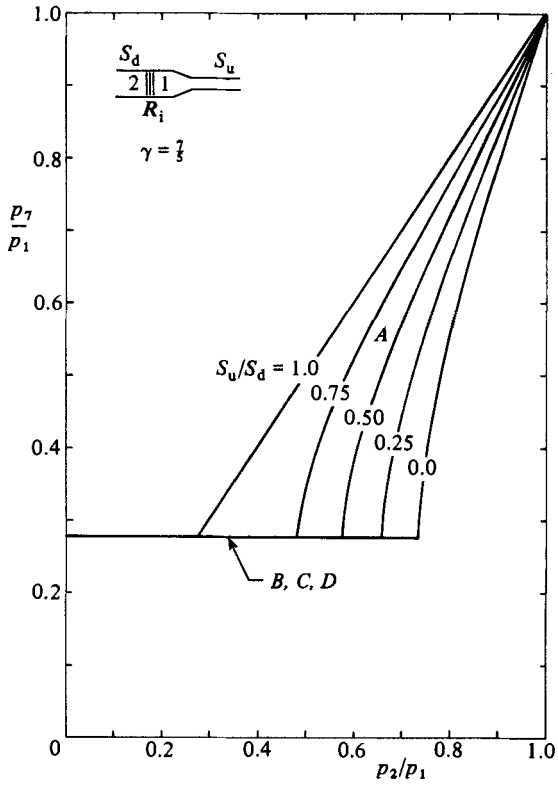

FIGURE 5. Strength of the transmitted rarefaction wave p_7/p_1 shown as a function of the incident rarefaction-wave strength p_2/p_1 and area-reduction ratio S_u/S_d, for perfect air and diatomic gases with with $\gamma = \frac{7}{5}$.

function of both p_2/p_1 and S_u/S_d. Also, the boundaries corresponding to wave patterns A to D are indicated by the dashed lines. For each given area ratio in the range $0 < S_u/S_d < 1$, a continuous variation in p_3/p_2 from unity to zero occurs through regions A to D as p_2/p_1 decreases from unity to zero. Over most of the range of S_u/S_d not too close to zero, p_3/p_2 is larger than p_2/p_1 and the reflected wave is weaker than the incident wave. The reverse situation occurs for very small values of S_u/S_d. For the case of no area change when $S_u/S_d = 1$, the reflected rarefaction wave is not present, because $p_3/p_2 = 1$, and only patterns A and D are possible as described previously. On the other hand, for the case when $S_u/S_d = 0$, one can show that $p_3/p_2 = [2-(p_1/p_2)^{(\gamma-1)/2\gamma}]^{2\gamma/(\gamma-1)}$ and only patterns A and B can occur. This corresponds to the case for which the incident wave is reflected from the closed end of a duct, since the flow from the duct of area S_u into the infinitely larger duct of area S_d has a negligible effect on the wave-reflection process. However, this relatively minor flow from the small to the large duct can be entirely subsonic and shock-wave free, as for pattern A, or partly supersonic and then subsonic after the stationary shock wave, as for pattern B.

It is interesting to observe that changes in p_2/p_1 produce relatively small changes in p_3/p_2 in region C of figure 6, whereas they produce relatively large changes in p_3/p_2 in region D. This behaviour is a direct result of the presence of the downstream-swept shock wave in pattern C and the downstream-swept rarefaction wave in pattern D.

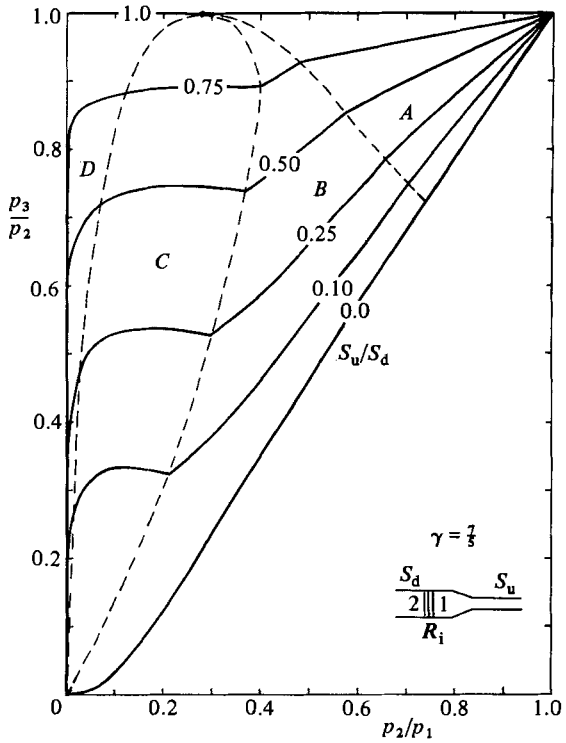

FIGURE 6. Strength of the reflected rarefaction wave p_3/p_2 shown as a function of the incident rarefaction-wave strength p_2/p_1 and area-reduction ratio S_u/S_d, for perfect air and diatomic gases with $\gamma = \frac{7}{5}$.

The shock wave causes an increase in pressure in region 3 of the wave pattern, whereas the rarefaction wave causes a decrease in pressure.

Finally, the strength p_5/p_6 of the stationary shock wave in pattern B and strengths p_5/p_6 and p_3/p_6 of the downstream-swept shock and rarefaction waves of patterns C and D respectively are shown in figure 7. For a given area ratio S_u/S_d and decreasing values of p_2/p_1, the stationary shock wave first appears with a strength $p_5/p_6 = 1$ at the lower boundary of region B, and its strength then rises monotonically to its maximum value at the boundary between regions B and C. For a further reduction in p_2/p_1 the strength p_5/p_6 of the downstream-swept shock wave decreases from this maximum value to unity at the boundary separating regions C and D. Thereafter, the strength p_3/p_6 of the downstream-swept rarefaction wave decreases rapidly in region D to zero as p_2/p_1 goes to zero.

3.2. *Non-stationary flow*

Numerical results obtained by the RCM for the interaction of a rarefaction wave with an area reduction are now presented graphically and discussed, in order to illustrate how the transmitted, reflected and other waves form, evolve with time, and eventually attain constant strengths as they become quasi-steady, in agreement with the quasi-steady flow predictions for the asymptotic wave patterns. Computations were made for many different combinations of the incident rarefaction-wave strength and area-reduction ratio; however, only a few typical results are presented here. Additional RCM results for perfect diatomic gases ($\gamma = \frac{7}{5}$), as well as additional

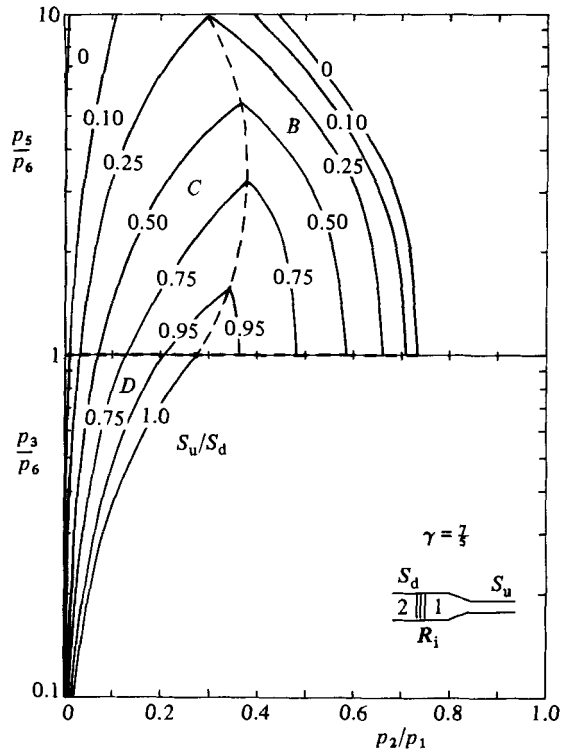

FIGURE 7. Strengths of the stationary shock wave of pattern B (p_5/p_6), and downstream-swept shock wave of pattern C (p_5/p_6), and downstream-swept rarefaction wave of pattern D(p_3/p_6), for perfect air and diatomic gases with $\gamma = \frac{7}{5}$.

quasi-steady flow solutions for perfect monatomic gases ($\gamma = \frac{5}{3}$), are presented graphically elsewhere (Gottlieb & Saito 1983).

The numerical results obtained with the RCM are given in figures 8–12, in the form of separate sets of spatial distributions for non-dimensional pressure p/p_1, flow velocity u/a_1, density ρ/ρ_1 and entropy $(s-s_1)/R$. Each successive distribution is displaced upward from the previous one, so that the effect of a time–distance diagram is produced. The non-dimensional time interval between adjacent distributions is given by $\Delta\tau = a_1 \Delta t/l$, and the non-dimensional value of $\Delta\tau$ for each case is given in the caption of each figure. The location of the area reduction of length l is shown by the two vertical dashed lines. The incident rarefaction wave is initially specified in the bottom distribution of each set, just to the left of the area reduction. In each case it is distributed over a distance of five-sixths of the length of the area change or $\frac{5}{6}l$. The initial flow velocity is specified to change linearly over this spatial interval, and the other flow properties can be derived from this variation and the specification of the incident rarefaction-wave strength p_2/p_1. Such a specification of the spatial properties of the incident rarefaction wave means that it was originally a centred rarefaction wave at some earlier distance and time. The flow field was computed with 720 grid zones, of which 60 were allocated to the area reduction and 50 are allocated to the incident rarefaction-wave profile.

The first set of numerical results for the pressure and flow velocity appears in figure 8, for the case of $p_2/p_1 = 0.65$ and $S_u/S_d = 0.75$, corresponding to a point in the upper domain for pattern A in figure 3. The incident rarefaction wave is shown in the bottom

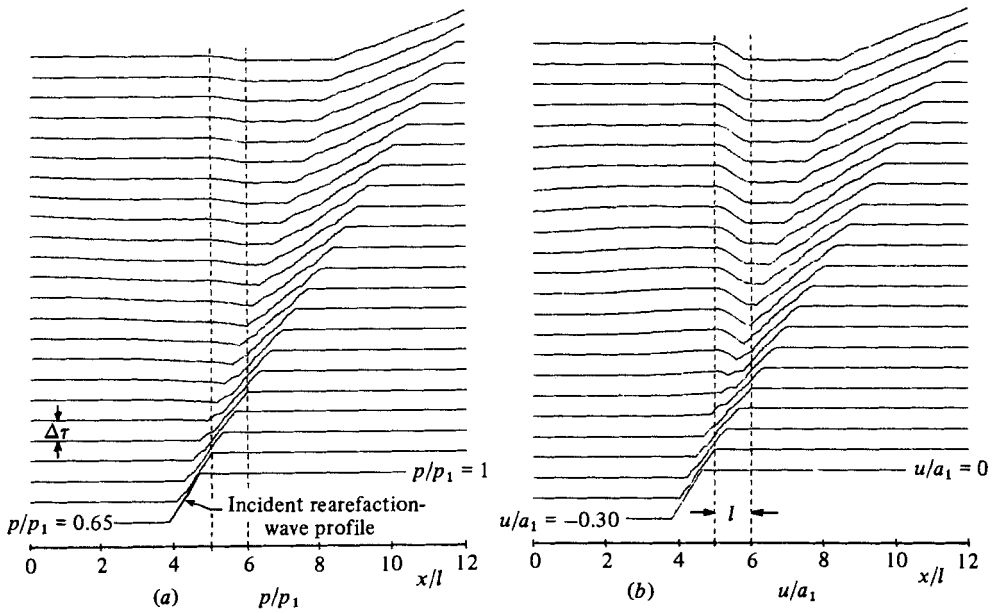

FIGURE 8. Spatial distributions of pressure (*a*) and flow velocity (*b*) for the interaction of a rarefaction wave with an area reduction ($p_2/p_1 = 0.65$, $S_u/S_d = 0.75$, $\Delta\tau = 0.34$, pattern *A*). Note that l is the length of the area reduction and $\Delta\tau = a_1 \Delta t/l$ is the non-dimensional time between successive spatial distributions.

distribution, just prior to its impingement on the area reduction. Its subsequent interaction can be observed in the following distributions, where the formation and evolution of the transmitted and reflected rarefaction waves, as well as the eventual development of steady subsonic flow in and on both sides of the area change, can be clearly seen. For the present case of a small area reduction, the reflected rarefaction wave is quite weak, relative to the incident wave, and barely noticeable. It would have been stronger and more visible if S_u/S_d had been lower than 0.75. Note that the steady flow in the area change at later times decelerates (velocity becomes less negative) and its pressure rises as the gas moves from right to left through an area enlargement. This is the expected flow behaviour for such a subsonic diffuser.

Other numerical results for different values of p_2/p_1 and S_u/S_d, corresponding to points in the upper part of the domain of pattern *A*, for which $S_u/S_d > 0.45$, are similar to those given in figure 8. However, numerical results for the lower part of this domain showed one interesting anomaly. A compression wave that might be initially smooth or have one or more coalescing shocks was found to form in the area change and then follow the tail of the transmitted rarefaction wave. This can be seen in the second set of results given in figure 9, for which $p_2/p_1 = 0.80$ and $S_u/S_d = 0.25$. In this case the pressure change $(p-p_1)/p_1$ across this compression wave with two coalescing shocks is about 0.08, which is not negligible when compared to the pressure changes of 0.20 and 0.35 across the incident and transmitted waves, respectively.

When the results shown in figure 9 were extended to later times (not shown), it was found that the compression wave with the two shocks steepened into one shock wave with one sharp front. This shock wave also overtook and interacted with the transmitted rarefaction wave. It was obvious that this interaction process would proceed slowly with time, continuously eroding the tail of the rarefaction wave and

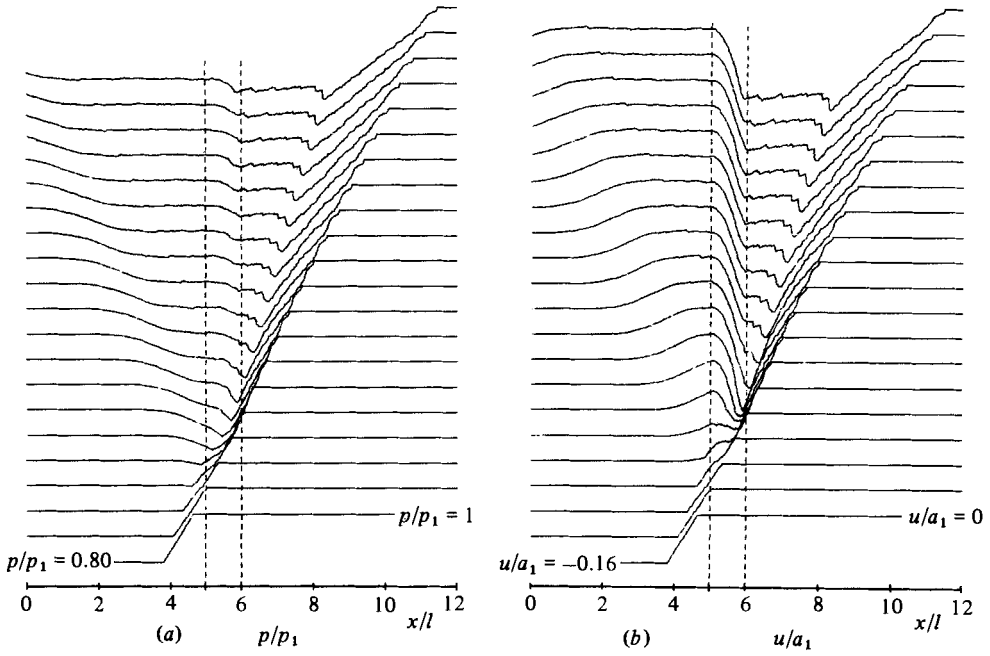

FIGURE 9. Spatial distributions of pressure (*a*) and flow velocity (*b*) for the interaction of a rarefaction wave with an area reduction ($p_2/p_1 = 0.80$, $S_u/S_d = 0.25$, $\Delta\tau = 0.34$, pattern *A*).

simultaneously reducing the strength of the overtaking shock wave, until only a weaker transmitted rarefaction wave is eventually left (Bremner, Dukowicz & Glass 1961). The final strength of this transmitted wave should then agree with the quasi-steady flow prediction.

It is worth pointing out that the formation of a compression wave which results in a steep-fronted shock wave at the tail of a rarefaction wave that is moving into an area convergence is not some new phenomenon, but rather a variation of a known feature of spherical explosions. For example, the sudden release of a high-pressure sphere of gas into its surroundings not only produces an outward-moving shock wave and inward-moving rarefaction wave, but also an imploding shock wave at the tail of the rarefaction wave (Saito & Glass 1979). This imploding shock wave, resulting from a steepening compression wave owing to the spherical geometry, reflects at the origin to form the second outward-moving shock wave. In the present problem, however, the final area convergence to a focus is absent. Hence, for sufficiently large area reductions for which a compression or shock wave forms behind the rarefaction wave, a transmitted rarefaction wave followed by a compression or shock wave should be expected.

It is apparent from the results presented in figures 8 and 9 that the wave pattern that emerges at late times is pattern *A*. This was also true of all other results for values of p_2/p_1 and S_u/S_d that correspond to points in the domain of quasi-steady wave pattern *A*, even for points taken very close to the boundary to pattern *B*. Furthermore, pattern *A* emerges fairly quickly in the numerical results, and the wave strengths converge fairly rapidly to those predicted by the quasi-steady flow analysis. This occurs shortly after the tail of the incident rarefaction wave enters the area change and shortly after the tails of the transmitted and reflected rarefaction waves

leave the vicinity of the area reduction, after which quasi-steady flow regions of increasing extent begin to develop on each side of the area change. The flow properties in these growing regions, as computed by the RCM, are generally within 5% of the quasi-steady flow predictions by the time that the tail of the last wave leaving the area change has moved approximately two area-transition lengths ($2l$) away from the area change. Also, at this time the strengths of the reflected and transmitted waves are within 5% of the quasi-steady flow predictions, except for the case when a compression or shock wave overtakes the transmitted wave. In such a case the strength of the transmitted wave will take a much longer time to decrease to within 5% of its final quasi-steady flow prediction.

The third set of numerical results for the pressure, flow velocity, density and entropy are presented in figure 10, for the case of $p_2/p_1 = 0.45$ and $S_u/S_d = 0.40$, corresponding to a point near the centre of the domain of pattern B. The first part of the incident rarefaction wave moves all of the way through the area reduction and establishes the transmitted rarefaction wave. The tail of this transmitted wave becomes stationary at the flow entrance to the area change where the flow becomes sonic, and no steady-flow region develops upstream of the area change. The latter part of the incident rarefaction wave cannot move through the area reduction, against the high-speed oncoming flow that is at least sonic at the flow entrance to the area change. However, this part of the incident wave produces a low pressure in the area change, and thus causes the flow to accelerate from sonic to increasing supersonic speeds as it passes through the area change, like the flow in a supersonic nozzle. Any compression wave that forms at the tail of the incident rarefaction wave as it moves into the area reduction would also be stalled by the high-speed oncoming flow. Consequently, a sufficiently strong upstream-facing shock wave develops in the area change and eventually becomes stationary near the centre (for the present case). It terminates the oncoming supersonic flow and a subsonic diffuser flow then follows in the downstream part of the area change. The reflected rarefaction wave in the present example is relatively weak compared to the incident wave, but it is visible in the numerical results.

During the formation of the upstream-facing shock wave a contact region of changing density and entropy is produced, which is swept downstream by the flow at the local flow velocity (see figures 10*c*, *d*). When the upstream-facing shock wave is stationary in the area change, it then produces a new quasi-steady flow region with a constant density and entropy between the contact region and area reduction. Note that the large fluctuations in the entropy distributions in figure 10(*d*) stem from the RCM. Small random variations in placing the upstream-facing shock wave in the area reduction lead to large entropy fluctuations. These random variations and thus the entropy fluctuations can be reduced by using a finer grid and/or a more appropriate random-number algorithm for the computations (Igra, Gottlieb & Saito 1983).

Numerical results computed for other incident rarefaction-wave strengths and area-reduction ratios corresponding to points in the domain of pattern B were similar to those given in figure 10. In each case the wave pattern that emerged at late times was always pattern B, even for points taken next to the boundaries to patterns A and C. Furthermore, quasi-steady wave pattern B emerges fairly quickly in the numerical results, but not as quickly as that for pattern A. Shortly after the tail of the incident wave enters the area reduction, the tail of the reflected wave leaves the area change and the upstream-facing shock wave becomes stationary. Shortly thereafter the flow becomes quasi-steady, with the wave amplitudes and the flow

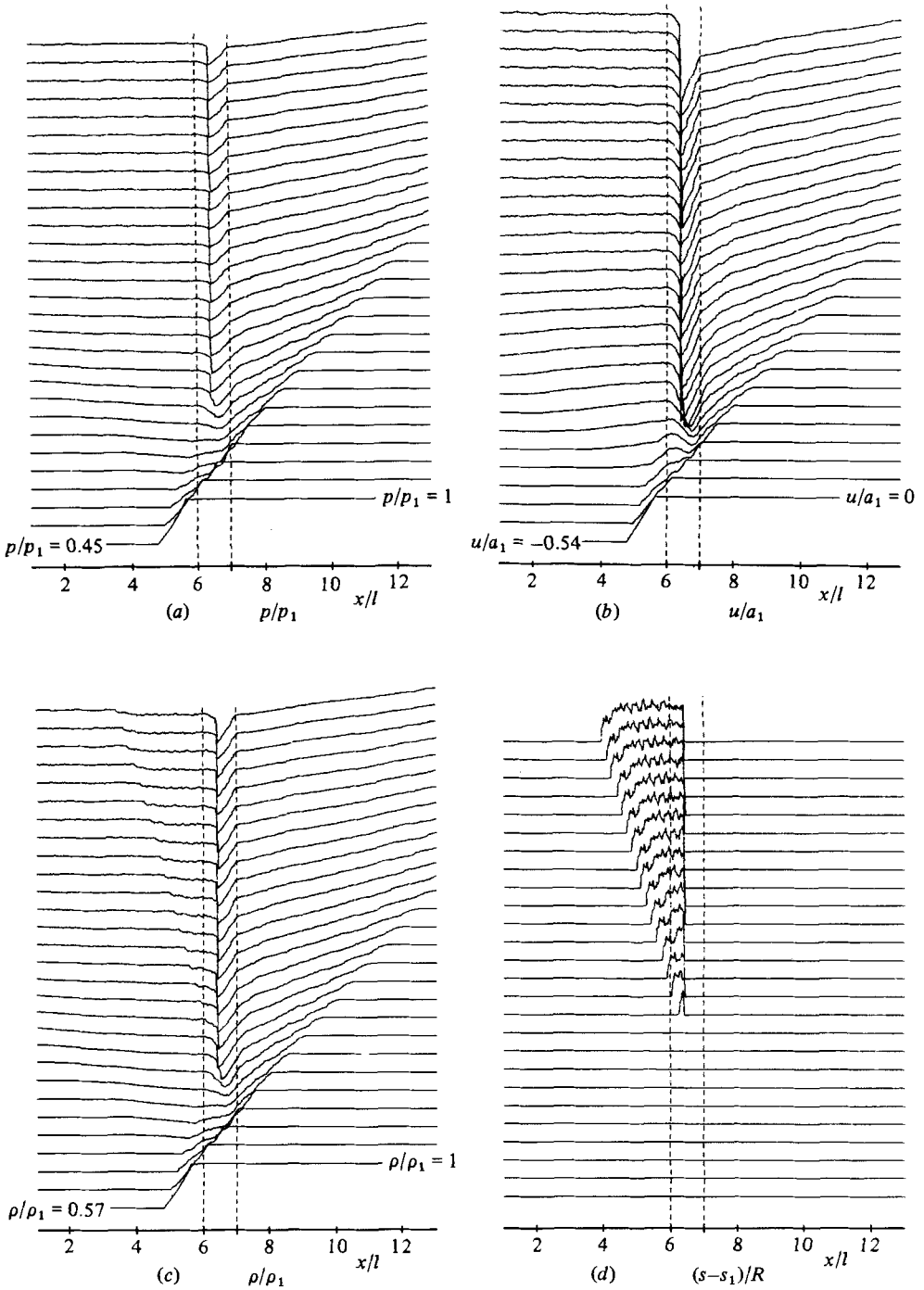

FIGURE 10. Spatial distributions of pressure (*a*), flow velocity (*b*), density (*c*) and entropy (*d*) for the interaction of a rarefaction wave with an area reduction ($p_2/p_1 = 0.45$, $S_u/S_d = 0.40$, $\Delta\tau = 0.48$, pattern *B*).

properties in the quasi-steady regions being within 5% of the predicted quasi-steady values.

The fourth set of numerical results for the pressure, flow velocity, density and entropy are presented in figure 11, for the case of $p_2/p_1 = 0.15$ and $S_u/S_d = 0.20$, corresponding to a point in the lower part of the domain of pattern C. As in the last case, the first part of the incident rarefaction wave moves through the area reduction and establishes the transmitted rarefaction wave with a stationary tail at the flow entrance to the area change. The centre part of the incident wave also reduces the pressure in the area reduction, such that an upstream-facing shock wave with a contact region is formed. However, in this case the additional, latter part of the strong incident rarefaction wave slowly overtakes the upstream-facing shock wave. This wave-interaction process results in a gradual weakening of the upstream-facing shock wave and the gradual disappearance of the overtaking rarefaction wave (Glass, Heuckroth & Molder 1961). As the shock wave weakens it is swept downstream by the oncoming supersonic flow, as shown in figure 11. For this particular case the wave interaction process will end when the tail of the incident rarefaction wave eventually overtakes the shock wave (not shown in the figure). A weaker upstream-facing but downstream-swept shock wave will then emerge with a constant strength. This was shown to be true for the present case, in spite of the lengthy time and high cost of the numerical calculations.

It should be clear from the numerical results given in figure 11 and their discussion that quasi-steady wave pattern C will eventually be established for the present case. Similar results were obtained for other incident rarefaction-wave strengths and area-reduction ratios corresponding to points in the domain of pattern C. The time required for pattern C to be established, however, is long relative to those times to establish patterns A and B, because the wave interaction process for the overtaking of the upstream-facing shock wave by the latter part of the incident rarefaction wave proceeds relatively slowly.

The final set of numerical results are presented in figure 12, for the case of $p_2/p_1 = 0.020$ and $S_u/S_d = 0.25$, corresponding to a point in the bottom part of the domain of pattern D. These results are typical for all other incident rarefaction-wave strengths and area-reduction ratios corresponding to points in the domain of pattern D. The flow development with time is similar to the previous case for pattern C, with one important exception. The incident rarefaction-wave strength is now sufficiently strong that the wave interaction process for the overtaking of the upstream-facing shock wave by the latter part of the incident rarefaction wave proceeds slowly to a different conclusion. The shock wave will gradually be reduced to a Mach wave (or eliminated) in the interaction process and a weaker upstream-facing rarefaction wave will eventually emerge with a constant strength (Glass *et al.* 1961). This is not shown in the results of figure 12, owing to the excessive time and cost required to continue the numerical calculations. However, it is clear from the figure that the shock-wave strength is diminishing with time and this shock wave is being swept downstream more quickly.

It is fairly obvious from these results and their discussion that quasi-steady wave pattern D will eventually be established when the incident rarefaction-wave strength and area-reduction ratio correspond to any point in the domain of wave pattern D. The time required for pattern D to be established, however, is long relative to that to establish pattern C, and even longer relative to those to establish patterns A and B. Note that the reason for the increase in the times to establish patterns A, B, C and D is that a sequence of events always occurs. Pattern A is always formed first.

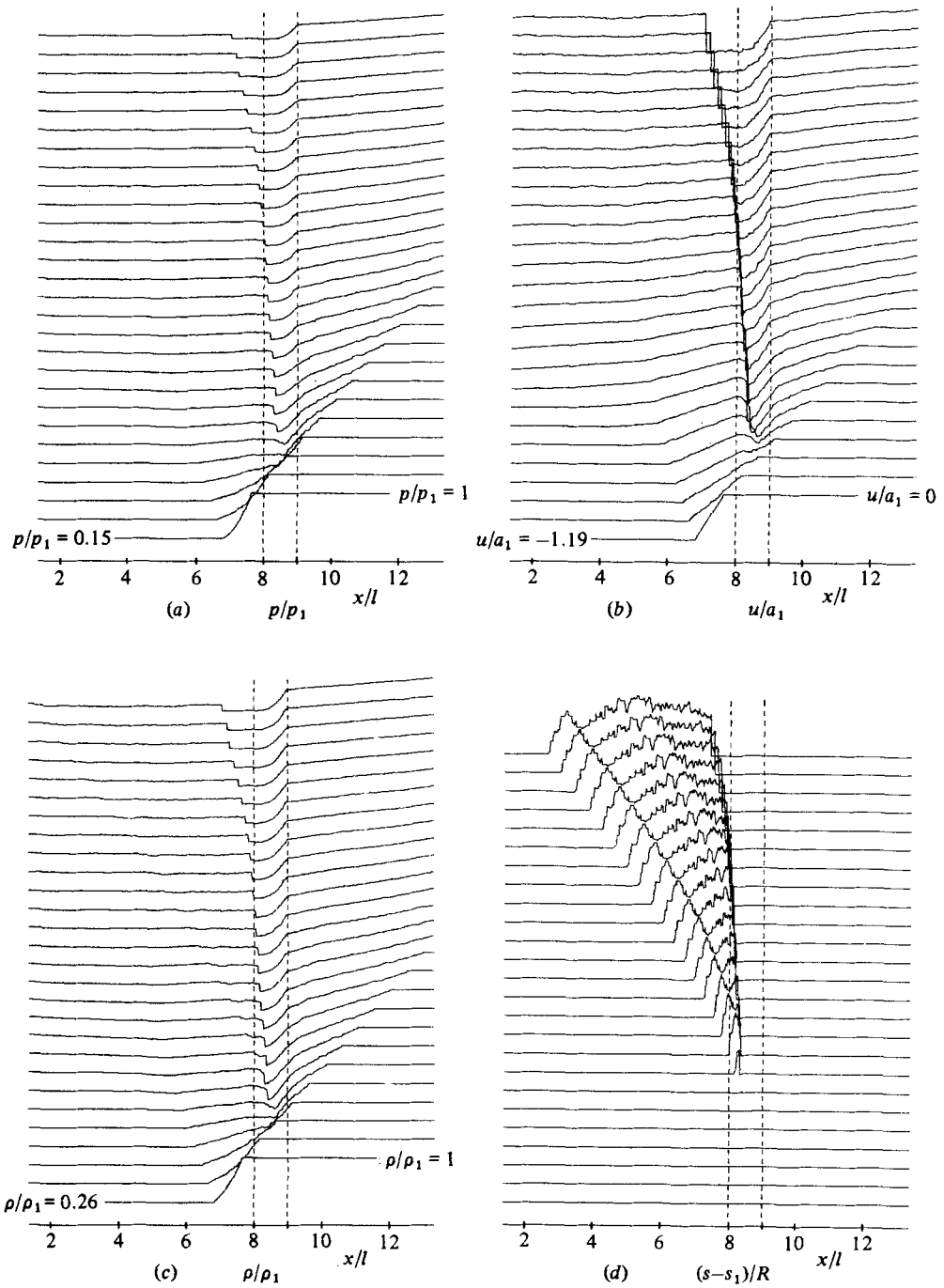

FIGURE 11. Spatial distributions of pressure (*a*), flow velocity (*b*), density (*c*) and entropy (*d*) for the interaction of a rarefaction wave with an area reduction ($p_2/p_1 = 0.15$, $S_u/S_d = 0.20$, $\Delta\tau = 0.49$, pattern *C*).

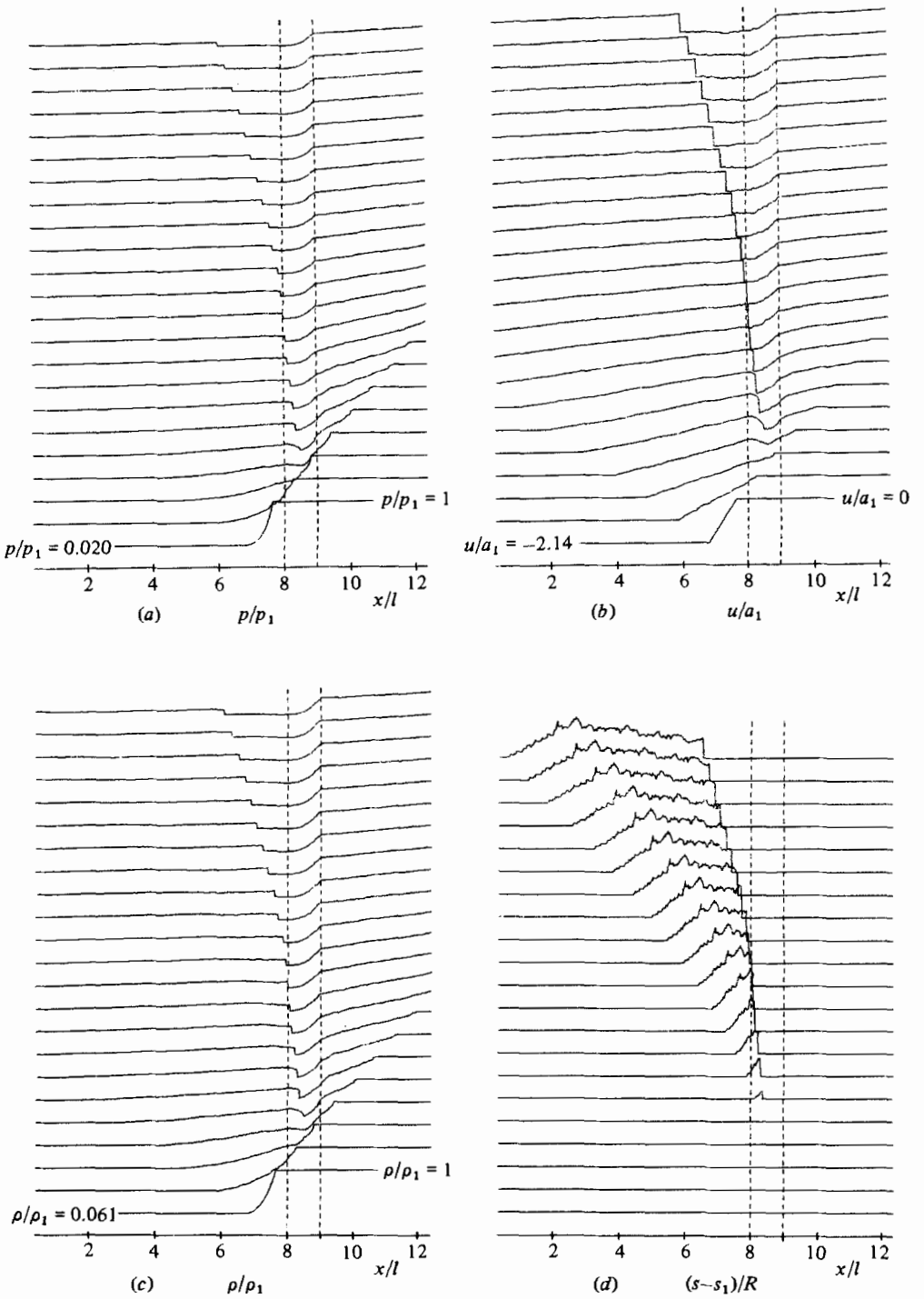

FIGURE 12. Spatial distributions of pressure (*a*), flow velocity (*b*), density (*c*) and entropy (*d*) for the interaction of a rarefaction wave with an area reduction ($p_2/p_1 = 0.020$, $S_u/S_d = 0.25$, $\Delta\tau = 0.62$, pattern *D*).

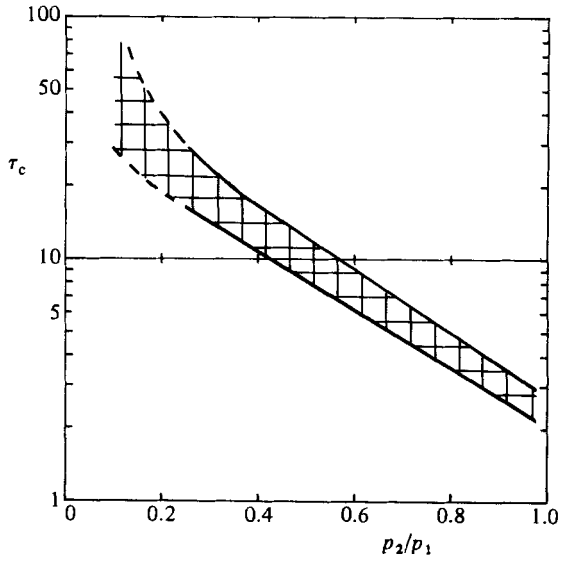

FIGURE 13. Characteristic time $\tau_c = a_1 t_c/l$ versus incident rarefaction-wave strength p_2/p_1 for the initially non-stationary flow eventually to become almost quasi-steady (within 5%).

If the rarefaction wave is sufficiently strong, pattern A is changed into pattern B, pattern B is then altered to pattern C, and pattern D finally evolves from pattern C.

The characteristic time for the non-stationary flow to become quasi-steady and establish pattern A, B, C or D has been discussed only qualitatively. In order to obtain quantitative results, a definition for this characteristic time is needed. Let the characteristic time t_c be defined as the time interval measured from when the incident rarefaction wave first encounters the area reduction until the non-stationary flow properties in 'quasi-steady' flow regions between distinct waves are within 5% of the quasi-steady flow predictions. Based on this definition, the non-dimensional characteristic time $\tau_c = a_1 t_c/l$ obtained from the numerical results are shown versus the incident rarefaction-wave strength in figure 13. The characteristic times (shown as a banded region) increase for stronger incident rarefaction waves or decreasing values of p_2/p_1. This should be expected because a stronger rarefaction wave with a wider fan of characteristics would take longer to complete its interaction with the area reduction.

The characteristic times are presented in the form of a banded region rather than a single curve or curves for the following two reasons. Firstly, the choice of a characteristic time from numerically predicted results for the non-stationary flow properties to come within 5% of the quasi-steady flow prediction is somewhat arbitrary, because the numerical results contain numerical noise or random fluctuations typical of the RCM. Hence precise values could not be obtained in the present work. Finally, the characteristic times were found to be weakly dependent on the area-reduction ratio, which could not be determined with precision from the numerical results. However, the trend was that characteristic times were always slightly longer for more severe area reductions, for a given value of p_2/p_1.

For the numerical results presented in figures 8–12 the spatial extent of the incident rarefaction wave was always taken to be five-sixths of the length of the area reduction. When the spatial extent of the incident wave was decreased, it was found

that the transient-flow behaviour did not change appreciably and the time to establish a particular pattern did not become significantly shorter. When the spatial extent was increased, however, it was found that the transient-flow behaviour was similar but extended proportionally in time.

4. Concluding remarks

The interaction of rarefaction waves with gradual, monotonic area reductions in ducts has been studied successfully with two complementary analyses. The quasi-steady flow analysis that describes the flow behaviour at late times was instrumental in establishing the asymptotic wave patterns, including the asymptotic values of the quasi-steady flow properties and the asymptotic strengths of the transmitted, reflected and other waves, as a function of the incident rarefaction-wave strength and area-reduction ratio. The non-stationary flow analysis was necessary for determining the transient flow behaviour from early to late times and showing how the quasi-steady flow was eventually established. The random-choice method was found to be excellent for solving this non-stationary flow problem.

The non-stationary flow analysis showed that the asymptotic wave patterns were established very rapidly for pattern A, quite rapidly for pattern B, and very slowly for pattern C and D (see figure 13). Consequently, the quasi-steady flow analysis would give a good estimate of the flow properties and the strengths of the transmitted, reflected and other waves at fairly early times for patterns A and B, but not for patterns C and D. For the cases of patterns C and D, or when a detailed study of the transient wave behaviour is needed, the non-stationary flow analysis is required to obtain accurate flow-field calculations.

In the present work the flow in the duct and area change has been assumed inviscid and one-dimensional for simplicity. The resulting flow calculations are, therefore, not always good approximations for actual flows in ducts. For example, actual flows through a large or rapid increase in area are normally two-dimensional with a thickening boundary layer, flow separation from the walls, and oblique upstream-facing shock waves if the flow is initially supersonic. Also, because the gas has been assumed perfect, real-gas effects like liquefaction at low temperatures behind strong rarefaction waves have been neglected. The reader is reminded of such limitations on the present work, even though these limitations are not given here in detail mainly for the sake of brevity.

Note that the complementary analytical and numerical study of the interaction of a rarefaction wave with an area enlargement has recently been completed, and it is available as a UTIAS report (Igra *et al.* 1983).

The authors would like to thank Dr T. Saito for his help in obtaining numerical results with the RCM, Mr P. Ostaff for his assistance with the quasi-steady flow computations, and Mr R. L. Deschambault for handling the word processing involved with the manuscript. The financial support received mainly from the Defence Research Establishment Suffield and partly from the Natural Sciences and Engineering Research Council, both of Canada, is much appreciated.

REFERENCES

BANNISTER, F. K. & MUCKLOW, G. F. 1948 Wave action following sudden release of compressed gas from a cylinder. *Proc. Indust. Mech. Engng* **159**, 269.

BREMNER, G. F., DUKOWICZ, J. K. & GLASS, I. I. 1961 One-dimensional overtaking of a rarefaction wave by a shock wave. *ARS J.* 1455. (Also *University of Toronto Inst. for Aerophys. UTIA Tech. Note* no. 33 (1960).)

CHESTER, W. 1960 The propagation of shock waves along ducts of varying cross section. *Adv. Appl. Mech.* **6**, 119.

CHORIN, A. J. 1976 Random choice solution of hyperbolic systems. *J. Comp. Phys.* **22**, 517.

GLASS, I. I., HEUCKROTH, L. E. & MOLDER, S. 1961 One-dimensional overtaking of a shock wave by a rarefaction wave. *ARS J.* 1453. (Also *University of Toronto Inst. for Aerophys. UTIA Tech. Note* no. 30 (1959).)

GLIMM, J. 1965 Solution in the large for nonlinear hyperbolic systems of equations. *Commun. Pure Appl. Maths* **18**, 697.

GOTTLIEB, J. J. & SAITO, T. 1983 An analytical and numerical study of the interaction of rarefaction waves with area changes in ducts – part 1: area reductions. *University of Toronto Inst. for Aerospace Studies UTIAS Rep.* no. 272.

GREATRIX, D. R. & GOTTLIEB, J. J. 1982 An analytical and numerical study of a shock wave interaction with an area change. *University of Toronto Inst. for Aerospace Studies UTIAS Rep.* no. 268.

IGRA, O., GOTTLIEB, J. J. & SAITO, T. 1983 An analytical and numerical study of the interaction of rarefaction waves with area changes in ducts – part 2: area enlargements. *University of Toronto Institute for Aerospace Studies UTIAS Rep.* no. 273.

JONES, A. D. & BROWN, G. L. 1982 Determination of two-stroke engine exhaust noise by the method of characteristics. *J. Sound Vib.* **82**, 305.

KAHANE, A., WARREN, W. R., GRIFFITH, W. C. & MARINO, A. A. 1954 A theoretical and experimental study of finite wave interactions with channels of varying area. *J. Aero. Sci.* **21**, 505.

RUDINGER, G. 1955 *Wave Diagrams for Nonstationary Flow in Ducts.* Van Nostrand. (Also *Nonsteady Duct Flow: Wave Diagram Analysis.* Dover (1969).)

RUSSELL, D. A. 1967 Shock-wave strengthening by area convergence. *J. Fluid Mech.* **27**, 306.

SAITO, T. & GLASS, I. I. 1979 Application of random-choice method to problems in shock and detonation-wave dynamics. *University of Toronto Inst. for Aerospace Studies UTIAS Rep.* no. 240.

SCHULTZ-GRUNOW, F. 1943 Nichtstationäre, kugelsymmetrische Gasbewegung und nichtstationäre Gasströmung in Dusen und Diffusoren. *Ing. Arch.* **14**, 21.

SOD, G. A. 1977 A numerical study of a converging cylindrical shock. *J. Fluid Mech.* **83**, 785.

WARMING, R. F. & BEAM, R. M. 1977 On the construction and application of implicit factored schemes for conservation laws. In *Proc. SIAM–AMS Symp. on Computational Fluid Dynamics, New York.*